HHS Public Access

Author manuscript

Cell Rep. Author manuscript; available in PMC 2021 January 08.

Published in final edited form as:

Cell Rep. 2020 November 24; 33(8): 108409. doi:10.1016/j.celrep.2020.108409.

Shigella flexneri Disruption of Cellular Tension Promotes Intercellular Spread

Jeffrey K. Duncan-Lowey[1,4], **Alexandra L. Wiscovitch**[2,5], **Thomas E. Wood**[1,3], **Marcia B. Goldberg**[1,3,*], **Brian C. Russo**[1,3,6,7,*]

[1]Center for Bacterial Pathogenesis, Division of Infectious Diseases, Department of Medicine, Massachusetts General Hospital, Boston, MA 02114, USA

[2]Research Scholar Initiative, The Graduate School of Arts and Sciences, Harvard University, Cambridge, MA 02138, USA

[3]Department of Microbiology, Blavatnik Institute, Harvard Medical School, Boston, MA 02115, USA

[4]Present address: Department of Immunobiology, Yale School of Medicine, New Haven, CT 06511, USA

[5]Present address: Department of Molecular Genetics and Microbiology, University of Florida, Gainesville, FL 32611, USA

[6]Present address: Department of Immunology and Microbiology, University of Colorado School of Medicine, Aurora, CO 80045, USA

[7]Lead Contact

SUMMARY

During infection, some bacterial pathogens invade the eukaryotic cytosol and spread between cells of an epithelial monolayer. Intercellular spread occurs when these pathogens push against the plasma membrane, forming protrusions that are engulfed by adjacent cells. Here, we show that IpaC, a *Shigella flexneri* type 3 secretion system protein, binds the host cell-adhesion protein β-catenin and facilitates efficient protrusion formation. *S. flexneri* producing a point mutant of IpaC that cannot interact with β-catenin is defective in protrusion formation and spread. Spread is restored by chemical reduction of intercellular tension or genetic depletion of β-catenin, and the magnitude of the protrusion defect correlates with membrane tension, indicating that IpaC reduces membrane tension, which facilitates protrusion formation. IpaC stabilizes adherens junctions and

*Correspondence: marcia.goldberg@mgh.harvard.edu (M.B.G.), brian.russo@cuanschutz.edu (B.C.R.).

AUTHOR CONTRIBUTIONS

This project was conceived of and experiments were designed by J.K.D.-L., M.B.G., and B.C.R. All experiments were performed by J.K.D.-L., A.L.W., T.E.W., and B.C.R. The manuscript was written by J.K.D.-L., A.L.W., T.E.W., M.B.G., and B.C.R.

SUPPLEMENTAL INFORMATION

Supplemental Information can be found online at https://doi.org/10.1016/j.celrep.2020.108409.

DECLARATION OF INTERESTS

The authors declare no competing interests.

does not alter β-catenin localization at the membrane. Thus, *Shigella*, like other bacterial pathogens, reduces intercellular tension to efficiently spread between cells.

Graphical Abstract

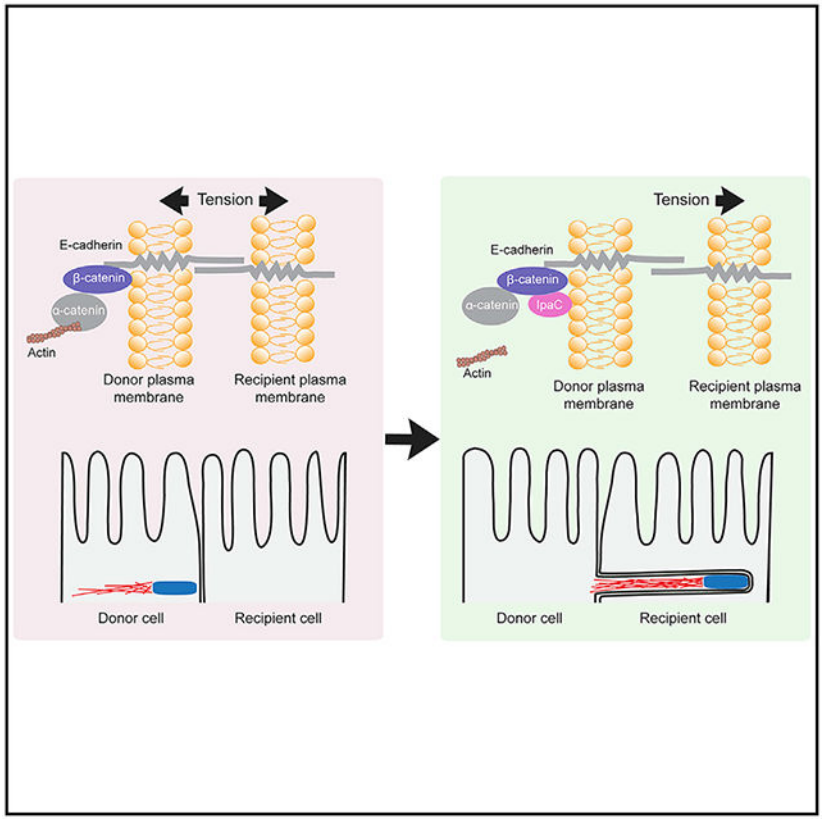

In Brief

Duncan-Lowey et al. show that the intracellular pathogen *Shigella flexneri* overcomes membrane tension during cell-to-cell spread by the type 3 secreted protein IpaC. The binding of IpaC to the host cell-adhesion protein β-catenin promotes the initiation of plasma membrane protrusions that enable the movement of bacteria into adjacent cells.

INTRODUCTION

Many cytosol-dwelling bacterial pathogens have evolved mechanisms of spreading directly from the cytosol of an infected cell (donor) into an uninfected adjacent cell (recipient). Intercellular spread enables pathogens to access new nutrients while avoiding immune clearance (Sansonetti et al., 1991; Weddle and Agaisse, 2018a). *Shigella flexneri*, an intracellular Gram-negative bacterial pathogen, infects colonic epithelial cells, replicates, and subsequently spreads between cells of the epithelium (Labrec et al., 1964; Sansonetti et al., 1986). Intercellular spread is required for *S. flexneri* to cause disease and efficiently colonize the host (Mitchell et al., 2020; Sansonetti et al., 1991; Yum et al., 2019). Cytosolic *S. flexneri* polymerizes actin and moves in a directed manner to the cell periphery

(Bernardini et al., 1989; Egile et al., 1999; Goldberg and Theriot, 1995), where it remodels the plasma membrane into pathogen-containing protrusions (Kadurugamuwa et al., 1991; Robbins et al., 1999). Bacterium-containing protrusions are engulfed into a vacuole by recipient cells in a clathrin-dependent process (Fukumatsu et al., 2012). Bacteria escape this vacuole into the cytosol of the donor cell (Allaoui et al., 1992; Campbell-Valois et al., 2015; Uchiya et al., 1995; Weddle and Agaisse, 2018b), which enables repeated cycles of intercellular spread through the epithelial monolayer. The forces derived from actin-based motility are necessary for protrusion formation (Monack and Theriot, 2001), whereas other pathogen and host factors, including the type 3 secretion translocon pore proteins IpaB and IpaC and the type 3 effectors OspE1/2, IcsB, and VirA, are required for efficient intercellular spread (Allaoui et al., 1995; Campbell-Valois et al., 2014, 2015; Heindl et al., 2010; Kuehl et al., 2014; Ogawa et al., 2003; Page et al., 1999; Schuch et al., 1999; Yi et al., 2014; Yoshida et al., 2006). Understanding the molecular mechanisms by which these proteins contribute to spread will define the parameters necessary for bacterial spread.

Here, we show that the efficient formation of plasma membrane protrusions and intercellular spread by *S. flexneri* is dependent upon IpaC. We show that IpaC binds to the cell-cell adhesion protein β-catenin and that the IpaC-β-catenin interaction enabled the efficient formation of membrane protrusions. Substitution of an arginine residue in the C-terminal tail of IpaC abrogated the interaction of IpaC with b-catenin and consequently diminished protrusion formation and spread. *Shigella* infection perturbed cell junctional configurations in a manner that depended upon IpaC binding to β-catenin. Chemical reduction of membrane tension or β-catenin depletion rescued *Shigella* spread. The efficiency of protrusion formation correlated with membrane tension, indicating that the interaction of IpaC with β-catenin enables the generation of protrusions by reducing cell-cell tension at sites of spread.

RESULTS

The IpaC C-Terminal Tail Is Required for Efficient Intercellular Spread of *S. flexneri*

During invasion by *S. flexneri*, the type 3 secreted protein IpaC interacts with intermediate filaments; this interaction is necessary for efficient bacterial docking onto host cells and for efficient translocation of effectors into the host cell cytosol (Russo et al., 2016). Because the type 3 secretion system (T3SS) and the secreted protein IpaC are also required for *S. flexneri* to spread between cells (Kuehl et al., 2014; Page et al., 1999; Schuch et al., 1999), we hypothesized that the interaction between IpaC and intermediate filaments might be required during spread. We tested the efficiency of spread for *S. flexneri* Δ*ipaC*-producing wild-type (WT) IpaC or an IpaC derivative that is unable to interact with intermediate filaments (IpaC R362W) (Harrington et al., 2006; Russo et al., 2016; Terry et al., 2008). IpaC R362W is efficiently secreted and, during invasion, forms normal-sized pores in the plasma membrane (Russo et al., 2016, 2019a). Bacterial plaques formed in monolayers of mouse embryonic fibroblasts (MEFs) were smaller for *S. flexneri* Δ*ipaC*-producing IpaC R362W than for *S. flexneri* Δ*ipaC*-producing WT IpaC (Figures 1A and 1B). The number of plaques is a function of the efficiency of bacterial invasion, whereas the size of plaques is a function of the efficiency of bacterial spread. Surprisingly, the absence of intermediate filaments did not

affect plaque size (Figures 1A and 1B), and the sizes of plaques formed by WT *S. flexneri* in $Vim^{+/+}$ and $Vim^{-/-}$ MEFs were not different (Figure 1C). Vimentin is the only intermediate filament expressed in these cells (Colucci-Guyon et al., 1994; Holwell et al., 1997). Bacteria producing WT IpaC or IpaC R362W replicate at similar efficiencies in broth culture (Figure S1A) and inside cells (Figures S1B and S1C), indicating that the reduction in plaque size is not attributable to differences in bacterial growth rate.

S. flexneri infects epithelial cells of the intestine, in which the predominant intermediate filaments are keratins rather than vimentin. As with MEFs (Figures 1A–1C), the plaques formed in monolayers of Caco-2 cells, which express keratins, were smaller for bacteria producing IpaC R362W than for bacteria producing WT IpaC (Figures 1D–1E). Also, as in MEFs, spread in Caco-2 cells occurred independent of intermediate filaments (Figures S2A–S2C). Altogether, these data show that the spread of *S. flexneri* is independent of intermediate filaments and dependent upon the presence of the IpaC R362.

IpaC Is Necessary for Efficient Formation of Plasma Membrane Protrusions

We assessed the efficiency of *S. flexneri* Δ*ipaC*-producing IpaC variants to form plasma membrane protrusions, an early step in intercellular spread. In HeLa cells, the percentage of intracellular bacteria located in membrane protrusions was markedly decreased for bacteria producing IpaC R362W, as compared to bacteria producing WT IpaC (Figures 2A and 2B), which demonstrates that IpaC is required for the formation of bacterium-containing membrane protrusions and that IpaC R362W is defective in this process. Given that forces derived from actin-based motility are required for the formation of membrane protrusions and, under heterologous experimental conditions, can be sufficient (Makino et al., 1986; Monack and Theriot, 2001), we hypothesized that bacteria producing IpaC R362W might be defective in actin-based motility. To evaluate the efficiency of actin-based motility, we tracked intracellular bacteria with actin tails by using live microscopy in HeLa cells stably producing GFP-tagged actin (LifeAct). There was no difference in the speed of *Shigella*-producing IpaC R362W and *Shigella*-producing WT IpaC (Figures 2C and 2D). Moreover, the percentage of bacteria producing IpaC R362W with an actin tail was not different from that of bacteria producing WT IpaC (Figures S3G–S3I).

In addition, defects in other early postentry processes were not observed (Figure S3). Bacteria producing IpaC R362W efficiently escaped from the vacuole into the cytosol (Figure S3B). They regulated effector secretion through the T3SS in a manner that is similar to WT IpaC both in the timing of effector secretion (Figures S3C and S3D) and in the magnitude of secretion activation (Figures S3C and S3E). Unlike an *icsB* mutant, they avoided recruitment of autophagy components similarly to bacteria producing WT IpaC (Figure S3F). Altogether, these data indicate that IpaC is required for the formation of plasma membrane protrusions and that *S. flexneri* Δ*ipaC*-producing IpaC R362W is impaired in spread due to a defect in its ability to form protrusions.

Cell-Cell Tension Is Reduced by *S. flexneri* in an IpaC-Dependent Manner

During infection by *Listeria monocytogenes* and *Rickettsia parkeri*, the secreted proteins Internalin C (*L. monocytogenes*) and Sca4 (*R. parkeri*) decrease cell-cell tension and enable

the formation or resolution of protrusions (Lamason et al., 2016; Rajabian et al., 2009). We hypothesized that IpaC may similarly facilitate protrusion formation by decreasing intercellular tension. To test this hypothesis, we measured junctional linearity of the plasma membrane during infection, as previously described (Otani et al., 2006). Cells with normal membrane tension have straight membranes between adjacent cell-cell vertices, whereas cells in which cell-cell membrane tension is decreased have membranes that are both more curved and longer between points of cell contact. This assay is sensitive to multiple parameters, including cell density; to control for experimental variability, we infected WT Caco-2 cells seeded at the same density and maintained under identical conditions. Caco-2 cells infected with bacteria producing WT IpaC had membranes that curved more than membranes of cells infected with bacteria producing IpaC R362W or uninfected cells (Figures 3A and 3B), indicating that *S. flexneri* decreases cell-cell tension in an IpaC-dependent fashion.

Because cell-cell tension at the adherens junction is maintained by the cortical actomyosin network , we tested whether the IpaC-mediated reduction of actomyosin-mediated tension is required for protrusion formation. To do so, we inhibited myosin II, which causes cell-cell tension to be relieved (Lamason et al., 2016; Rajabian et al., 2009). In HeLa cells, treatment with the myosin II inhibitor blebbistatin fully rescued protrusion formation of *S. flexneri* that produces IpaC R362W (Figures 3C and 3D) but did not affect protrusion formation by bacteria producing WT IpaC, demonstrating that protrusion formation requires IpaC-mediated reduction in membrane tension.

The membrane tension of cells is inversely proportional to their density in a monolayer (Nehls et al., 2019). We therefore hypothesized that the role of IpaC R362 in protrusion formation might be more pronounced in sub-confluent cells than in confluent cells. As with HeLa cells (Figures 2A and 2B) and MEFs (Figure S3I), protrusion formation in Caco-2 monolayers was more efficient for bacteria producing WT IpaC than for bacteria producing IpaC R362W (Figures 3E and 3F). Consistent with our hypothesis, bacteria were present in protrusions at higher rates in confluent cells (Figure 3F) than in sub-confluent cells (Figure 3E), and the relative defect in protrusion formation for bacteria producing IpaC R362W was less in confluent cells than in sub-confluent cells (Figures 3E and 3F). Altogether, these data indicate that IpaC reduces membrane tension in a manner that promotes protrusion formation.

S. flexneri Spread Requires an Interaction of IpaC with β-Catenin

Catenin-cadherin networks maintain cell-cell tension and are integral for protecting against membrane stress (Ray et al., 2013). Because IpaC interacts with the cell-cell adhesion protein β-catenin (Shaikh et al., 2003), a component of these catenin-cadherin networks, we hypothesized that the disruption of cell-cell tension by IpaC may depend on its interaction with β-catenin and that IpaC R362 may be required for this interaction. To assess the efficiency of β-catenin binding to IpaC variants, we used a yeast-based protein-protein interaction assay (de Groot et al., 2011; Russo et al., 2016; Schmitz et al., 2009; Yi et al., 2014). In this assay, a prey protein is tagged with mCherry and a bait protein is fused to the reovirus scaffold protein μNS, which forms inclusions bodies within the yeast cytosol

(Schmitz et al., 2009). The protein-protein interaction results in the formation of fluorescent puncta, and in the absence of an interaction, the mCherry signal is generally diffuse throughout the cell (Figure 4A). Co-expression of IpaC-mCherry and β-catenin-μNS resulted in fluorescent puncta in most yeast, whereas co-expression of IpaC R362W-mCherry and β-catenin-μNS resulted in diffuse mCherry signal with few puncta (Figures 4B and 4C). As noted previously, some yeast display background fluorescent foci in the absence of an interacting partner (Russo et al., 2016; Schmitz et al., 2009). IpaC folds normally in yeast, as puncta formation is observed when IpaC-mCherry is expressed with μNS fused to IpaC's chaperone IpgC but not with μNS alone (Figure S4A). Thus, IpaC interacts with β-catenin, and this interaction requires IpaC R362.

We tested the impact of β-catenin depletion on the efficiency of *S. flexneri* spread in both HeLa and Caco-2 cells. In both cell types, β-catenin is predominantly localized to the membrane (Figure S4B), consistent with its role in adherens junctions. Knockdown of β-catenin in both HeLa cells and Caco-2 cells rescued the spread of *S. flexneri* Δ*ipaC*-producing IpaC R362W (Figures 4D and 4E; Figures S4C–S4G). As expected, in cells expressing a scrambled short hairpin RNA (shRNA), *S. flexneri* Δ*ipaC*-producing IpaC R362W spread less efficiently than bacteria producing WT IpaC (Figures 4D and 4E; Figure S4G). Consistent with previous findings (Ray et al., 2013), knockdown of β-catenin on its own is not sufficient to alter membrane linearity (Figure S3F), indicating that additional stresses associated with bacterial infection or other bacterial proteins are likely required to reduce membrane tension. Previous work has shown that γ-catenin, also known as plakoglobin, has some functional redundancy with β-catenin and, under conditions in which cells experience relatively little stress, can compensate for knockdown of β-catenin (Ray et al., 2013; Wickline et al., 2013). These data demonstrate that β-catenin is a negative regulator of *S. flexneri* intercellular spread and that the interaction of IpaC with β-catenin disrupts β-catenin function in membrane tension.

IpaC Stabilizes Adherens Junctions at the Membrane

At membranes, β-catenin interacts with type I cadherins (N-, M-, and E-cadherin), which links α-catenin and cortical actin to the membrane (Drees et al., 2005). The type of cadherin expressed varies by cell type; Caco-2 cells express E-cadherin, whereas fibroblasts and HeLa cells express N-cadherin (Figure S5A). IpaC and E-cadherin interact with the same region of β-catenin (Figure S5B; Huber and Weis, 2001; Shaikh et al., 2003). The cytoplasmic tails of N- and E-cadherin are similar (Figure S5C), and both cadherins interact with β-catenin. We hypothesized that the interaction of IpaC with β-catenin might disrupt the interaction of β-catenin with cadherin, thereby uncoupling the connection to the actin cytoskeleton. To test this hypothesis, we visualized the localization of β-catenin during infection with *S. flexneri* Δ*ipaC*-producing WT IpaC or IpaC R362W in Caco-2 cells. β-catenin remained localized to the membrane during infection; it was not observed to be recruited to cytoplasm-dwelling bacteria, and it did not accumulate in cell nuclei (Figure 5A). Previous reports showed that β-catenin localized with bacterial protrusions and actin tails (Sansonetti et al., 1994); in our assays, β-catenin localized at approximately 90% of protrusions (Figures 5A–5C), and β-catenin localization to protrusions was similar for bacteria producing WT IpaC and bacteria producing IpaC R362W. β-catenin recruitment

was similar for protrusions from confluent and sub-confluent cells (Figures 5B and 5C). β-Catenin localization in the membrane fraction was unaltered by infection, with minimal amounts of β-catenin present in either the nucleus or cytoplasm (Figure 5D). Other components of the adherens junction, α-catenin and N-cadherin, also remained localized to the membrane during infection (Figure 5D). The subcellular distribution of these molecules was similar for HeLa cells infected with bacteria producing WT IpaC, those infected with bacteria producing IpaC R362W, and uninfected cells (Figure 5D). Vinculin was predominantly in the cytoplasm, with or without infection (Figure 5D).

To further explore the influence of IpaC on the interaction of cadherins with β-catenin, we examined these interactions in the yeast-based protein interaction assay (Figure 5E). The interaction of β-catenin with cadherin was increased in the presence of WT IpaC and, yet, was not altered by the presence of IpaC R362W (Figures 5F and 5G). Expression of IpaC R362W had no impact on the efficiency of the cadherin-β-catenin interaction, as the interaction was similar to that of no IpaC (Figures 5F and 5G). Together, these data show that IpaC alters the β-catenin-cadherin interaction without causing β-catenin to delocalize from the membrane.

DISCUSSION

For cytosol-dwelling bacterial pathogens, direct spread from an initially infected cell into an adjacent cell is essential for dissemination and disease pathogenesis. To traverse the plasma membranes, bacteria remodel the cellular cortical cytoskeleton. Here, we show that the *S. flexneri* protein IpaC decreases cell-cell tension, promotes the formation of plasma membrane protrusions, and enables intercellular spread. Membrane tension was dissipated by the binding of IpaC to the cell-cell adhesion protein β-catenin.

For efficient spread, *S. flexneri* must simultaneously maintain cell-cell contacts but release membrane tension. Several cell-cell adhesion proteins, including cadherin, tricellulin, and occludin, are required for efficient intercellular spread by *S. flexneri* (Fukumatsu et al., 2012; Sansonetti et al., 1994); these proteins contribute to the maintenance of intercellular connections during the process of spread. Our finding that β-catenin restricts bacterial spread appears to oppose the role of E-cadherin in promoting spread. We speculate that the interaction of IpaC with β-catenin generates slack membranes while maintaining sufficient homotypic interactions of E-cadherin molecules to maintain cell-cell contact. The stabilization of β-catenin with E-cadherin could maintain E-cadherin at the membrane and tether the membrane closer to the bacteria, which might enable more efficient and directed actin-based propulsion. Thus, by targeting catenin-cadherin interactions by β-catenin, IpaC may selectively alter the activity of the cadherin complex while not disrupting cadherin-dependent cell-cell contact.

One possibility is that the IpaC interaction with β-catenin could alter the composition of adherens junctions in a manner that alters membrane tension and facilitates *Shigella* intercellular spread. To regulate membrane tension, the cellular adhesion protein α-catenin rapidly switches between binding to β-catenin and to cortical actin. The increased affinity of

β-catenin for E-cadherin in the presence of IpaC could regulate β-catenin/α-catenin interactions and thus alter membrane tension.

The adherens junction component α-catenin regulates the polymerization of actin, which could modify the motility of actively spreading bacteria. It was previously found that actin within the tails of motile cytosolic *Shigella* is polymerized by Arp2/3 but that in the protrusion, bacterial actin polymerization switches to a formin-dependent process (Heindl et al., 2010). α-Catenin acts as a molecular switch that regulates the switch to formin-dependent polymerization (Drees et al., 2005). If IpaC-β-catenin complexes were to increase the concentration of membrane-bound α-catenin, then this could facilitate the switch to formin-dependent actin polymerization near the bacteria.

At different stages of *S. flexneri* infection, the arginine immediately adjacent to the C terminus of IpaC (R362) is required for interactions with two distinct cellular proteins where it participates in two distinct functions. In addition to being required for the formation of protrusions during intercellular spread, IpaC R362 is required for interactions with intermediate filaments to support docking during bacterial entry (Russo et al., 2016). Whether the binding preference of IpaC is determined by the distinct subcellular niche of the bacterium at these two stages of infection or by other factors is at present unclear. Of note, other *S. flexneri* type 3 secreted proteins have domains that bind more than one host protein; for example, during entry, vinculin binding site 3 of IpaA separately binds talin and vinculin (Valencia-Gallardo et al., 2019).

Like *S. flexneri, R. parkeri* and *L. monocytogenes* reduce cell-cell tension but do so by targeting host proteins distinct from those bound by *S. flexneri* IpaC. *R. parkeri* prevents vinculin-mediated cell tension by the type 4 secretion system effector protein Sca4, whereas the secreted *L. monocytogenes* protein Internalin C decreases cell-cell tension by binding the focal adhesion protein Tuba (Lamason et al., 2016; Rajabian et al., 2009). These findings provide evidence of convergent evolution by a cadre of pathogens upon mechanisms to decrease membrane tension and underscore that the plasma membrane is a critical barrier that must be subverted for successful bacterial infection.

STAR★METHODS

RESOURCE AVAILABILITY

Lead Contact—Further information and requests for resources and reagents should be directed to and will be fulfilled by the Lead Contact, Brian Russo (brian.russo@cuanschutz.edu).

Materials Availability—Materials, including plasmids and strains, are available from the authors upon request.

Data and Code Availability—The published article includes the data generated in this study, no unique software or code were generated for this study.

EXPERIMENTAL MODEL AND SUBJECT DETAILS

Bacterial Culture—The wild-type *S. flexneri* strain used in this study is *S. flexneri* 2457T (Labrec et al., 1964), and all mutants were isogenic derivatives of it. *S. flexneri* strains were cultured in trypticase soy broth at 37°C. *ipaC* derivatives were cloned into the plasmid pBAD33, and their expression was driven from the pBAD promoter, induced with 1.2% arabinose.

Cell Lines—HeLa, Caco-2, and MEFs were maintained at 37°C in 5% CO_2. All cells were grown in Dulbecco's modified Eagle's medium (DMEM) supplemented with 10% fetal bovine serum (FBS). Wild-type and vimentin knock-out MEFs were previously described (Styers et al., 2004). Caco-2 cells producing membrane-YFP (gift of Hervé Agaisse) and HeLa cell lines stably expressing t-farnesyl-RFP (gift of Rebecca Lamason), as well as Caco-2 and HeLa cells producing shRNAs targeting β-catenin [Broad Institute; TRCN000314921 andTRCN000314991(Yang et al., 2011)], or a control (Addgene, Cat# 10879; (Moffat and Sabatini, 2006) were generated using retroviral transduction with selection with 10 μg/ml puromycin.

METHOD DETAILS

Analysis of bacterial growth in broth—Overnight cultures of bacteria were diluted to an OD_{600} of 0.03 in TCS broth with appropriate antibiotics and 1.2% arabinose. 185 μL of diluted bacteria or media alone were added to a 96-well flat bottom plate. Six technical replicates were performed for each condition. Absorbance at 600nm was monitored every 10 min using a BioTeK Epoc2 plate reader with the chamber heated to 37°C and the plate shaken between readings.

Plaque Assays—For confluent monolayers, 8×10^5 (Caco-2) or 6×10^5 (MEF) cells per well were seeded in six-well plates. The next day, monolayers were infected with bacteria in mid-exponential phase at a multiplicity of infection (MOI) of 0.002 for MEFs and a MOI of 0.02 for Caco-2 cells in DMEM. In Figure 2C, the multiplicity of infection (MOI) was adjusted to compensate for the known decrease in efficiency of invasion by *S. flexneri* in the absence of interaction of IpaC with intermediate filaments. Bacteria were centrifuged onto cells at 800 ×*g* for 10 minutes and incubated at 37°C in 5% CO_2 for 50 minutes. Media was replaced with 0.5% agarose in DMEM with 25 μg/mL gentamicin, 10% FBS, 1.2% arabinose (for *ipaC* expression from the arabinose promoter), and 0.45% glucose and incubated an additional two days. An additional overlay was added, formulated as before but with 0.7% agarose and 0.1% neutral red. Following incubation for at least 4h, the plates were imaged with an Epson Perfection 4990 photo scanner. ImageJ was used to quantify plaque area. Within an experiment, plaques were thresholded to remove background, pixel intensity was saturated, and the images were segmented into objects. Objects matching plaques on an unmodified image were selected and their area was quantified by ImageJ.

Quantification of intracellular bacteria—HeLa cells were seeded at 4×10^5 cells per well in a 6-well plate. The next day they were infected at a MOI of 100. The bacteria were centrifuged onto the cells at 800 × *g* for 10 min at room temperature. The culture was incubated at 37°C with 5% CO_2 for 50 min. Excess bacteria were removed by three

successive washed with HBSS. Any remaining extracellular bacteria were killed by incubation of the infection in DMEM supplemented with 25 μg/mL gentamicin, in addition to 10% FBS, 1.2% arabinose. The infection was incubated for an additional 1, 2 or 3 hours. The cells were washed 3 times with HBSS, and then the HeLa cells were lysed with 0.02% SDS in HBSS. The HeLa cells lysates with intact bacteria were serially diluted and plated to determine the intracellular CFU.

Protrusion Assays—MEFs were seeded at 2×10^5 cells per well on coverslips or HeLa cells expressing t-farnesyl-RFP were seeded at 6×10^5 cells per well on coverslips and were infected the following day. Caco-2 cells expressing membrane-YFP were seeded at 4×10^5 cells per well and cultured for at least 3 days on glass coverslips prior to infection. Cells were infected at an MOI of 100, as above, with designated strains expressing pROEX-Aqua [Addgene; plasmid #42889, (Erard et al., 2013)]. At 30 minutes of infection, media was replaced with DMEM supplemented with 0.45% glucose, 1.2% arabinose, 25 μg/mL gentamicin, 20 mM IPTG, and 10% FBS. After an additional 3 hours, cells were fixed with 3.7% paraformaldehyde in PBS and stained with for 5 minutes with 1:10,000 Hoechst 33342 in PBS. Coverslips were mounted with Prolong Diamond Antifade Mountant and imaged the next day.

Live-cell Imaging Analysis—HeLa cells expressing *LifeAct-GFP* were seeded at 6×10^5 cells per well on 20 mm MatTek glass bottom dishes. The next day cells were infected at a MOI of 100, as above, with *S. flexneri* expressing a constitutive RFP and a GFP reporter of T3SS activity (pTSAR). At 30 minutes of infection, media was replaced with DMEM supplemented with 0.45% glucose, 1.2% arabinose, 25 μg/mL gentamicin, 50 mM HEPES, and 10% FBS. Samples were imaged with a Nikon Eclipse TE-300 at 37°C at 5 s intervals for 5 minutes. To calculate actin-tail mediated velocities, the ImageJ plugin particle tracker was used to track in-frame bacteria over the course of the video. Speed was determined for each bacterium by measuring the distance traveled over the duration of time the bacteria was in focus.

Membrane Linearity Assay—Membrane linearity was performed as previously described (Rajabian et al., 2009). Caco-2 cells were seeded onto fibronectin treated coverslips at a density of 8×10^5 cells per well and grown for 7 days to polarize the cells. After 4 days, the media was changed daily. Cells were infected as above with *S. flexneri* strains expressing the uropathogenic *E. coli* Afa-1 pilus (Labigne-Roussel et al., 1984), which binds to decay accelerating factor (CD55) on the surface of human cells (Nowicki et al., 1993) and enhanced infection at a MOI of 10. At 30 minutes of infection, media was replaced with DMEM, supplemented with 0.45% glucose, 1.2% arabinose, 25 μg/mL gentamicin, and 10% FBS. After an additional 3 hours, cells were fixed with 3.7% paraformaldehyde in PBS, permeabilized with 0.5% Triton X-100 in PBS, and stained with mouse anti-ZO-1 antibody (Invitrogen, cat# 339100; 1:100 dilution) and Alexa Fluor 568 conjugated secondary, with anti-*Shigella* antibody (ViroStat cat# 0903; 1:100 dilution), and with Hoechst 33342. Coverslips were mounted with Prolong Diamond Antifade Mountant and imaged the next day. The junction length was determined by measuring with ImageJ the linear distance between cell vertices and the actual length of the plasma membrane between

the same vertices. Junction length was expressed as a ratio of the actual length of the membrane divided by the linear inter-vertex distance.

Yeast Protein-Protein Interaction Assay—Yeast protein interaction assays were performed as previously described (Schmitz et al., 2009). To test the interaction of IpaC with β-catenin, yeast carried plasmids encoding mCherry-tagged IpaC variants and μNS alone (negative control) or μNS-tagged β-catenin. To test effect of IpaC on interaction of E-cadherin with β-catenin, yeast carried plasmids encoding IpaC variants, mNS-tagged β-catenin, and GFP tagged E-cadherin. As controls the empty vectors were also included. Yeast were cultured overnight in complete synthetic media lacking histidine and leucine supplemented with 2% raffinose. The next morning, strains were back diluted to OD_{600} 0.5 and grown for 2h at 30°C with 2% raffinose. Then, to induce protein synthesis, the media was changed to 2% galactose, and growth was allowed to proceed for 4 hours at 30°C. Yeast were wet mounted and imaged. The percentage of fluorescent yeast displaying a punctum was quantified.

Infectious Foci Assay—HeLa cells were seeded at a density of 6×10^5 cells per well on coverslips in 6 well plates. The next day, cells were infected as above at a MOI of 0.05 with designated strains. At 50 minutes of infection, media was replaced with DMEM supplemented with 0.45% glucose, 1.2% arabinose, 25 μg/mL gentamicin, and 10% FBS. Cells were incubated at 37°C with 5% CO_2 for 18 hours at which point they were rinsed once and fixed with 3.7% paraformaldehyde in PBS for 20 minutes. Cells were washed three times with PBS, incubated with 1 M glycine in PBS for 15 minutes, washed three additional times with PBS and then permeabilized with 0.5% Triton X-100 for 20 minutes. Cells were washed five times with PBS and incubated overnight at 4°C with Alexa Fluor 488 conjugated anti-*Shigella* antibody (ViroStat, 1:1000 dilution). Cells were washed three times with PBS, stained with Hoechst 33342, washed twice with PBS and mounted with Prolong Diamond Antifade Mountant. Foci were randomly imaged across the coverslip, and the number of infected cells within each focus was determined by counting nuclei that co-localized with bacteria.

Vacuolar Escape—The resistance of intracellular bacteria to chloroquine, which accumulates within vacuoles and kills intra-vacuolar bacteria but remains at sub-bactericidal concentrations within the cytosol, was tested as previously described (Zychlinsky et al., 1994). Notably, IpaC is an important factor in vacuolar escape (Du et al., 2016), Briefly, 1×10^4 $Vim^{+/+}$ MEFs were seeded into wells of a 96-well plate. The next day, cells were infected as above at a MOI of 100 with designated strains. At 50 minutes of infection, media was replaced with DMEM supplemented with 0.45% glucose, 1.2% arabinose, 25 μg/mL gentamicin, 10% FBS ± 200 μg/mL chloroquine. After 1 hour, cells were washed three times and lysed with 1% Triton X-100 in PBS. Bacteria were serially diluted 1:5 and the number of intracellular bacteria were enumerated by plating dilutions. Percent cytosolic bacteria were the ratio of colony forming units (CFU) in the presence of gentamicin and chloroquine to CFU in the presence of gentamicin without chloroquine multiplied by 100.

LC3 Co-localization—To quantify intracellular bacteria associated with LC3, HeLa cells stably expressing a GFP-LC3 construct were seeded at a density of 4×10^5 cells per well in a 6-well plate on coverslips (Conway et al., 2013). The next day, cells were infected as above at a MOI of 100 with indicated strains. At 50 minutes of infection, media was replaced with DMEM supplemented with 0.45% glucose, 1.2% arabinose, 25 μg/mL gentamicin, and 10% FBS. After an additional 3 hours, cells were washed once with PBS, fixed with 3.7% paraformaldehyde and stained with Hoechst 33342. Coverslips were mounted with Prolong Diamond Antifade Mountant, and cells were imaged randomly across the coverslip. LC3-positive bacteria were counted as those that co-localized with strong GFP signal.

Type 3 Secretion System Activity—To measure type 3 secretion system activity, Vim $^{+/+}$ MEFs were seeded at a density of 4×10^5 cells per well in 6-well plates on coverslips. The next day, cells were infected, as above, with indicated strains carrying the plasmid pTSAR [GFP expression is driven by the mxiE box, which requires type 3-mediated secretion of the effector OspD1, and mCherry is driven by the constitutive rpsM promoter (Campbell-Valois et al., 2014; Parsot et al., 2005). At 20 minutes of infection, media was replaced with DMEM supplemented with 0.45% glucose, 1.2% arabinose, 25 μg/mL gentamicin, and 10% FBS. At indicated time points, cells were washed once with PBS, fixed with 3.7% paraformaldehyde, and stained with Hoechst 33342. Cells were washed twice and mounted with Prolong Diamond Antifade Mountant. Cells were randomly imaged across the coverslip, and the percent of bacteria with active type 3 secretion systems was determined by enumerating the ratio of GFP-positive bacteria (T3SS active) to RFP-positive bacteria (total). To determine the intensity of GFP signal, bacteria were identified by an RFP signal, and the intensity of GFP signal was measured with imageJ (Schneider et al., 2012).

Actin Tail Formation—To quantify actin-tail formation, Vim$^{+/+}$ MEFs were seeded at a density of 4×10^5 cells per well in 6-well plates on coverslips. The next day, cells were infected as above with indicated strains. At 50 minutes of infection, media was replaced with DMEM supplemented with 0.45% glucose, 1.2% arabinose, 25 μg/mL gentamicin, and 10% FBS. After an additional 3 hours, cells were washed once with PBS, fixed with 3.7% paraformaldehyde, and stained with anti-*Shigella* antibody conjugated to Alexa Fluor 488 (ViroStat, 1:1000 dilution). The next day, cells were washed three times with PBS and stained with phalloidin conjugated to Alexa Fluor 568 (Invitrogen, cat# A12380). Cells were washed three times with PBS and stained with Hoechst 33342. Cells were washed twice more with PBS and mounted with Prolong Diamond Antifade Mountant. The percentage of bacteria with actin-tails was determined by counting the number of total bacteria (Alexa Fluor 488-positive) to the number of bacteria with actin-tails.

β-catenin localization—For immunofluorescent localization of β-catenin, HeLa cells or Caco-2 cells were seeded at 4×10^5 cells per well and cultured for 48 hours (HeLa) or 72 hours (Caco-2). Following fixation with PFA, the cells were permeabilized with 1% Triton X-100 for 30 minutes at room temperature. The cells were washed five times with PBS, blocked for 30 minutes at room temperature with 10% goat serum in PBS, and then incubated overnight at 1:500 of mouse anti-β-catenin in 10% goat serum in PBS. The cells were washed with PBS, incubated with 1:750 goat anti-mouse conjugated with either Alexa

Fluor 568 or Alexa Fluor 488 for 2 hours at room temperature and washed with PBS. The DNA was stained with Hoechst 33342, the cells were washed twice with PBS, and the coverslips were mounted with ProLong Diamond Antifade Mountant.

For subcellular localization of β-catenin by cellular fractionation, we used a detergent fraction method as has been done previously (Russo et al., 2016,2019a, 2019b; Scherer et al., 2000). Briefly, 4×10^5 cells were seeded in 6 well plates, four wells per condition. After 48 hours, cells were infected with a MOI of 100. The bacteria were centrifuged onto the cells at 800 × *g* at room temperature and incubated at 37°C for 50 min. The cells were washed with HBSS, the media was changed to DMEM supplemented with 0.45% glucose, 1.2% arabinose, 25 μg/mL gentamicin, and 10% FBS, and the cells were incubated for an additional 2 hours at 37C. The cells were washed three times with 50 mM Tris, pH 7.5. 0.5 mL per well of 50 mM Tris, pH 7.5 supplemented with protease inhibitors (Roche) was added to each well and the cells were scraped. The recovered cells were pelleted at 3,000 × *g* for 3 min at room temperature, the pellets from each well were pooled and washed with 50 mM Tris, pH 7.5. The pellet was incubated for 20 min in cold 0.2% saponin in 50 mM Tris, pH 7.5 150 mM NaCl and protease inhibitors. The cells were pelleted at 21,000 × *g* for 30 min at 4°C. The supernatant (the cytosol) was collected and the pellet was resuspended in cold 0.5% Triton X-100 in 50 mM Tris, pH 7.5 150 mM NaCl and protease inhibitors (Roche, Cat# 11836170001) and incubated for 30 min on ice. Samples were pelleted at 21,000 x *g* for 15 min at 4°C. The supernatant (the membrane fraction) was collected and the pellet contained cellular debris, intact bacteria, and intact nuclei. β-catenin abundance in the cellular fractions was determined by western blot.

Western Blots—Western blots were performed using 1:10,000 mouse anti-β-catenin (BD Biosciences, 610153), 1:1000 mouse anti-vinculin (Sigma, SAB4200729), or 1:1000 rat anti-N-cadherin [Developmental Studies Hybridoma Bank, MNCD2, (Matsunami and Takeichi, 1995)], 1:1000 rat anti-E-cadherin (Thermo, 14-3249-82) incubating overnight at 4°C, or 1:500 rabbit anti-α-catenin (Thermo, 71-1200), 1:1000 rabbit anti-caveolin 1 (Sigma, C4490), 1:1,000,000 rabbit anti-GroEL (Sigma, G6532), 1:1000 mouse anti-GAPDH (Developmental Studies Hybridoma Bank, DSHB-hGAPDH-2G7), 1:40,000 rabbit anti-keratin 8 (Abcam, Ab53280), 1:10,000 rabbit anti-keratin 18 (Abcam, ab668) 1:5000 goat anti-rabbit HRP (JacksonImmuno, 111-035-144), 1:5000 goat anti-rat HRP (JacksonImmuno, 112-035-003), and 1:5000 goat anti-mouse HRP (JacksonImmuno, 115035003) for 2 hours at room temperature. Western blots were developed, and signal was acquired by exposure to film. To determine band density, film was digitized using an Epson Perfection 4990 photo scanner and band intensity was measured using ImageJ.

Microscopy—Fluorescent images were acquired on either a Nikon TE300 or a Nikon TE-2000. Both are equipped with Chroma Technology filters, Q-imaging EXI Blue cameras, and use IVision 4.5 software (BioVision Technologies). Microscopic images were pseudo colored and assembled using Adobe Photoshop or ImageJ. Unless otherwise noted, images were collected in a random manner across the coverslip. For analysis of protrusions in Caco-2 cells, areas with bacteria were identified in the CFP channel and the edge of monolayers was determined by Hoechst staining. A minimum of five Z stacks was collected

per region on each coverslip with a 0.25 μM distance between slices. All bacteria in a stack were analyzed. To display representative images with protrusions, all slices within a stack containing the protrusion were collapsed into a single image based upon the maximum intensity of the pixels in each slice using ImageJ.

QUANTIFICATION AND STATISTICAL ANALYSIS

Statistical differences between means was determined with GraphPad Prism. Statistical differences between two means was tested by unpaired Student's t test. Differences between the means of three or more groups was tested by either two-way ANOVA with Sidak post hoc test or a one-way ANOVA with Tukey post hoc test or Dunnet's post hoc test.

Supplementary Material

Refer to Web version on PubMed Central for supplementary material.

ACKNOWLEDGMENTS

We thank Ramnik Xavier, Victor Faundez, and Claude Parsot for reagents. We thank Cammie Lesser, Amy Barczak, Hervé Agaisse, Rebecca Lamason, and Allen Sanderlin for reagents and helpful discussions. We thank the members of the Goldberg, Lesser, and Barczak laboratories for helpful discussions. We thank Natasha Bitar and Luisa Stamm for technical support and Brianna Lowey for helpful discussion and critical reading of the manuscript.

This work was funded by NIH grant AI081724 to M.B.G. and by NIH grants AI007061, AI137296, and AI114162, the Massachusetts General Hospital Executive Committee on Research Tosteson Award, and the Charles A. King Trust Postdoctoral Research Fellowship Program, Bank of America, N.A., Co-Trustees, to B.C.R.

REFERENCES

Allaoui A, Mounier J, Prévost MC, Sansonetti PJ, and Parsot C (1992). icsB: a *Shigella flexneri* virulence gene necessary for the lysis of protrusions during intercellular spread. Mol. Microbiol 6, 1605–1616. [PubMed: 1495389]

Allaoui A, Sansonetti PJ, Ménard R, Barzu S, Mounier J, Phalipon A, and Parsot C (1995). MxiG, a membrane protein required for secretion of *Shigella* spp. Ipa invasins: involvement in entry into epithelial cells and in intercellular dissemination. Mol. Microbiol 17, 461–470. [PubMed: 8559065]

Baxt LA, and Goldberg MB (2014). Host and bacterial proteins that repress recruitment of LC3 to *Shigella* early during infection. PLoS One 9, e94653. [PubMed: 24722587]

Bernardini ML, Mounier J, d'Hauteville H, Coquis-Rondon M, and Sansonetti PJ (1989). Identification of icsA, a plasmid locus of *Shigella flexneri* that governs bacterial intra- and intercellular spread through interaction with F-actin. Proc. Natl. Acad. Sci. USA 86, 3867–3871. [PubMed: 2542950]

Campbell-Valois FX, Schnupf P, Nigro G, Sachse M, Sansonetti PJ, and Parsot C (2014). A fluorescent reporter reveals on/off regulation of the *Shigella* type III secretion apparatus during entry and cell-to-cell spread. Cell Host Microbe 15, 177–189. [PubMed: 24528864]

Campbell-Valois FX, Sachse M, Sansonetti PJ, and Parsot C (2015). Escape of Actively Secreting *Shigella flexneri* from ATG8/LC3-Positive Vacuoles Formed during Cell-To-Cell Spread Is Facilitated by IcsB and VirA. MBio 6, e02567–14. [PubMed: 26015503]

Colucci-Guyon E, Portier MM, Dunia I, Paulin D, Pournin S, and Babinet C (1994). Mice lacking vimentin develop and reproduce without an obvious phenotype. Cell 79, 679–694. [PubMed: 7954832]

Conway KL, Kuballa P, Song JH, Patel KK, Castoreno AB, Yilmaz OH, Jijon HB, Zhang M, Aldrich LN, Villablanca EJ, et al. (2013). Atg16l1 is required for autophagy in intestinal epithelial cells and protection of mice from *Salmonella* infection. Gastroenterology 145, 1347–1357. [PubMed: 23973919]

de Groot JC, Schlüter K, Carius Y, Quedenau C, Vingadassalom D, Faix J, Weiss SM, Reichelt J, Standfuss-Gabisch C, Lesser CF, et al. (2011). Structural basis for complex formation between human IRSp53 and the translocated intimin receptor Tir of enterohemorrhagic *E. coli*. Structure 19, 1294–1306. [PubMed: 21893288]

Drees F, Pokutta S, Yamada S, Nelson WJ, and Weis WI (2005). Alpha-catenin is a molecular switch that binds E-cadherin-beta-catenin and regulates actin-filament assembly. Cell 123, 903–915. [PubMed: 16325583]

Du J, Reeves AZ, Klein JA, Twedt DJ, Knodler LA, and Lesser CF (2016). The type III secretion system apparatus determines the intracellular niche of bacterial pathogens. Proc. Natl. Acad. Sci. USA 113, 4794–4799. [PubMed: 27078095]

Egile C, Loisel TP, Laurent V, Li R, Pantaloni D, Sansonetti PJ, and Carlier MF (1999). Activation of the CDC42 effector N-WASP by the *Shigella flexneri* IcsA protein promotes actin nucleation by Arp2/3 complex and bacterial actin-based motility. J. Cell Biol 146, 1319–1332. [PubMed: 10491394]

Erard M, Fredj A, Pasquier H, Beltolngar DB, Bousmah Y, Derrien V, Vincent P, and Merola F (2013). Minimum set of mutations needed to optimize cyan fluorescent proteins for live cell imaging. Mol. Biosyst 9, 258–267. [PubMed: 23192565]

Fukumatsu M, Ogawa M, Arakawa S, Suzuki M, Nakayama K, Shimizu S, Kim M, Mimuro H, and Sasakawa C (2012). *Shigella* targets epithelial tricellular junctions and uses a noncanonical clathrin-dependent endocytic pathway to spread between cells. Cell Host Microbe 11, 325–336. [PubMed: 22520461]

Goldberg MB, and Theriot JA (1995). *Shigella flexneri* surface protein IcsA is sufficient to direct actin-based motility. Proc. Natl. Acad. Sci. USA 92, 6572–6576. [PubMed: 7604035]

Harrington A, Darboe N, Kenjale R, Picking WL, Middaugh CR, Birket S, and Picking WD (2006). Characterization of the interaction of single tryptophan containing mutants of IpaC from *Shigella flexneri* with phospholipid membranes. Biochemistry 45, 626–636. [PubMed: 16401091]

Heindl JE, Saran I, Yi CR, Lesser CF, and Goldberg MB (2010). Requirement for formin-induced actin polymerization during spread of *Shigella flexneri*. Infect. Immun 78, 193–203. [PubMed: 19841078]

Holwell TA, Schweitzer SC, and Evans RM (1997). Tetracycline regulated expression of vimentin in fibroblasts derived from vimentin null mice. J. Cell Sci 110, 1947–1956. [PubMed: 9296393]

Huber AH, and Weis WI (2001). The structure of the beta-catenin/E-cadherin complex and the molecular basis of diverse ligand recognition by beta-catenin. Cell 105, 391–402. [PubMed: 11348595]

Kadurugamuwa JL, Rohde M, Wehland J, and Timmis KN (1991). Intercellular spread of *Shigella flexneri* through a monolayer mediated by membranous protrusions and associated with reorganization of the cytoskeletal protein vinculin. Infect. Immun 59, 3463–3471. [PubMed: 1910001]

Kuehl CJ, Dragoi AM, and Agaisse H (2014). The *Shigella flexneri* type 3 secretion system is required for tyrosine kinase-dependent protrusion resolution, and vacuole escape during bacterial dissemination. PLoS One 9, e112738. [PubMed: 25405985]

Labigne-Roussel AF, Lark D, Schoolnik G, and Falkow S (1984). Cloning and expression of an afimbrial adhesin (AFA-I) responsible for P blood group-independent, mannose-resistant hemagglutination from a pyelonephritic *Escherichia coli* strain. Infect. Immun 46, 251–259. [PubMed: 6148308]

Labrec EH, Schneider H, Magnani TJ, and Formal SB (1964). Epithelial cell penetration asan essential step in the pathogenesis of bacillary dysentery. J. Bacteriol 88, 1503–1518. [PubMed: 16562000]

Lamason RL, Bastounis E, Kafai NM, Serrano R, Del Alamo JC, Theriot JA, and Welch MD (2016). Rickettsia Sca4 Reduces Vinculin-Mediated Intercellular Tension to Promote Spread. Cell 167, 670–683.e610. [PubMed: 27768890]

Makino S, Sasakawa C, Kamata K, Kurata T, and Yoshikawa M (1986). A genetic determinant required for continuous reinfection of adjacent cells on large plasmid in *S. flexneri* 2a. Cell 46, 551–555. [PubMed: 3524856]

Matsunami H, and Takeichi M (1995). Fetal brain subdivisions defined by R- and E-cadherin expressions: evidence for the role of cadherin activity in region-specific, cell-cell adhesion. Dev. Biol 172, 466–478. [PubMed: 8612964]

Mitchell PS, Roncaioli JL, Turcotte EA, Goers L, Chavez RA, Lee AY, Lesser CF, Rauch I, and Vance RE (2020). NAIP-NLRC4-deficient mice are susceptible to shigellosis. eLife 9, e59022. [PubMed: 33074100]

Moffat J, and Sabatini DM (2006). Building mammalian signalling pathways with RNAi screens. Nat. Rev. Mol. Cell Biol 7, 177–187. [PubMed: 16496020]

Monack DM, and Theriot JA (2001). Actin-based motility is sufficient for bacterial membrane protrusion formation and host cell uptake. Cell. Microbiol 3, 633–647. [PubMed: 11553015]

Nehls S, Nöding H, Karsch S, Ries F, and Janshoff A (2019). Stiffness of MDCK II Cells Depends on Confluency and Cell Size. Biophys. J 116, 2204–2211. [PubMed: 31126583]

Nowicki B, Hart A, Coyne KE, Lublin DM, and Nowicki S (1993). Short consensus repeat-3 domain of recombinant decay-accelerating factor is recognized by *Escherichia coli* recombinant Dr adhesin in a model of a cell-cell interaction. J. Exp. Med 178, 2115–2121. [PubMed: 7504058]

Ogawa M, Suzuki T, Tatsuno I, Abe H, and Sasakawa C (2003). IcsB, secreted via the type III secretion system, is chaperoned by IpgA and required at the post-invasion stage of *Shigella* pathogenicity. Mol. Microbiol 48, 913–931. [PubMed: 12753186]

Otani T, Ichii T, Aono S, and Takeichi M (2006). Cdc42 GEF Tuba regulates the junctional configuration of simple epithelial cells. J. Cell Biol 175, 135–146. [PubMed: 17015620]

Page AL, Ohayon H, Sansonetti PJ, and Parsot C (1999). The secreted IpaB and IpaC invasins and their cytoplasmic chaperone IpgC are required for intercellular dissemination of *Shigella flexneri*. Cell. Microbiol 1, 183–193. [PubMed: 11207551]

Parsot C, Ageron E, Penno C, Mavris M, Jamoussi K, d'Hauteville H, Sansonetti P, and Demers B (2005). A secreted anti-activator, OspD1, and its chaperone, Spa15, are involved in the control of transcription by the type III secretion apparatus activity in *Shigella flexneri*. Mol. Microbiol 56, 1627–1635. [PubMed: 15916611]

Rajabian T, Gavicherla B, Heisig M, Müller-Altrock S, Goebel W, Gray-Owen SD, and Ireton K (2009). The bacterial virulence factor InlC perturbs apical cell junctions and promotes cell-to-cell spread of Listeria. Nat. Cell Biol 11, 1212–1218. [PubMed: 19767742]

Ray S, Foote HP, and Lechler T (2013). beta-Catenin protects the epidermis from mechanical stresses. J. Cell Biol 202, 45–52. [PubMed: 23816618]

Robbins JR, Barth AI, Marquis H, de Hostos EL, Nelson WJ, and Theriot JA (1999). *Listeria monocytogenes* exploits normal host cell processes to spread from cell to cell. J. Cell Biol 146, 1333–1350. [PubMed: 10491395]

Russo BC, Stamm LM, Raaben M, Kim CM, Kahoud E, Robinson LR, Bose S, Queiroz AL, Herrera BB, Baxt LA, et al. (2016). Intermediate filaments enable pathogen docking to trigger type 3 effector translocation. Nat. Microbiol 1, 16025. [PubMed: 27572444]

Russo BC, Duncan JK, and Goldberg MB (2019a). Topological Analysis of the Type 3 Secretion System Translocon Pore Protein IpaC following Its Native Delivery to the Plasma Membrane during Infection. mBio 10, e00877–19. [PubMed: 31138750]

Russo BC, Duncan JK, Wiscovitch AL, Hachey AC, and Goldberg MB (2019b). Activation of *Shigella flexneri* type 3 secretion requires a host-induced conformational change to the translocon pore. PLoS Pathog. 15, e1007928. [PubMed: 31725799]

Sansonetti PJ, Ryter A, Clerc P, Maurelli AT, and Mounier J (1986). Multiplication of *Shigella flexneri* within HeLa cells: lysis of the phagocytic vacuole and plasmid-mediated contact hemolysis. Infect. Immun 51, 461–469. [PubMed: 3510976]

Sansonetti PJ, Arondel J, Fontaine A, d'Hauteville H, and Bernardini ML (1991). OmpB (osmo-regulation) and icsA (cell-to-cell spread) mutants of *Shigella flexneri*: vaccine candidates and probes to study the pathogenesis of shigellosis. Vaccine 9, 416–422. [PubMed: 1887672]

Sansonetti PJ, Mounier J, Prevost MC, and Mège RM (1994). Cadherin expression is required for the spread of *Shigella flexneri* between epithelial cells. Cell 76, 829–839. [PubMed: 8124719]

Scherer CA, Cooper E, and Miller SI (2000). The *Salmonella* type III secretion translocon protein SspC is inserted into the epithelial cell plasma membrane upon infection. Mol. Microbiol 37, 1133–1145. [PubMed: 10972831]

Schmitz AM, Morrison MF, Agunwamba AO, Nibert ML, and Lesser CF (2009). Protein interaction platforms: visualization of interacting proteins in yeast. Nat. Methods 6, 500–502. [PubMed: 19483691]

Schneider CA, Rasband WS, and Eliceiri KW (2012). NIH Image to ImageJ: 25 years of image analysis. Nat. Methods 9, 671–675. [PubMed: 22930834]

Schuch R, Sandlin RC, and Maurelli AT (1999). A system for identifying post-invasion functions of invasion genes: requirements for the Mxi-Spa type III secretion pathway of Shigella flexneri in intercellular dissemination. Mol. Microbiol 34, 675–689. [PubMed: 10564508]

Shaikh N, Terajima J, and Watanabe H (2003). IpaC of *Shigella* binds to the C-terminal domain of beta-catenin. Microb. Pathog 35, 107–117. [PubMed: 12927518]

Styers ML, Salazar G, Love R, Peden AA, Kowalczyk AP, and Faundez V (2004). The endo-lysosomal sorting machinery interacts with the intermediate filament cytoskeleton. Mol. Biol. Cell 15, 5369–5382. [PubMed: 15456899]

Terry CM, Picking WL, Birket SE, Flentie K, Hoffman BM, Barker JR, and Picking WD (2008). The C-terminus of IpaC is required for effector activities related to Shigella invasion of host cells. Microb. Pathog 45, 282–289. [PubMed: 18656530]

Uchiya K, Tobe T, Komatsu K, Suzuki T, Watarai M, Fukuda I, Yoshikawa M, and Sasakawa C (1995). Identification of a novel virulence gene, virA, on the large plasmid of *Shigella*, involved in invasion and intercellular spreading. Mol. Microbiol 17, 241–250. [PubMed: 7494473]

Valencia-Gallardo C, Bou-Nader C, Aguilar-Salvador DI, Carayol N, Quenech'Du N, Pecqueur L, Park H, Fontecave M, Izard T, and Tran Van Nhieu G (2019). Shigella IpaA Binding to Talin Stimulates Filopodial Capture and Cell Adhesion. Cell Rep. 26, 921–932.e926. [PubMed: 30673614]

Weddle E, and Agaisse H (2018a). Principles of intracellular bacterial pathogen spread from cell to cell. PLoS Pathog. 14, e1007380. [PubMed: 30543716]

Weddle E, and Agaisse H (2018b). Spatial, Temporal, and Functional Assessment of LC3-Dependent Autophagy in *Shigella flexneri* Dissemination. Infect. Immun 86, e00134–18. [PubMed: 29844234]

Wickline ED, Du Y, Stolz DB, Kahn M, and Monga SP (2013). γ-Catenin at adherens junctions: mechanism and biologic implications in hepatocellular cancer after β-catenin knockdown. Neoplasia 15, 421–434. [PubMed: 23555187]

Yang X, Boehm JS, Yang X, Salehi-Ashtiani K, Hao T, Shen Y, Lubonja R, Thomas SR, Alkan O, Bhimdi T, et al. (2011). A public genome-scale lentiviral expression library of human ORFs. Nat. Methods 8, 659–661. [PubMed: 21706014]

Yi CR, Allen JE, Russo B, Lee SY, Heindl JE, Baxt LA, Herrera BB, Kahoud E, MacBeath G, and Goldberg MB (2014). Systematic analysis of bacterial effector-postsynaptic density 95/disc large/zonula occludens-1 (PDZ) domain interactions demonstrates *Shigella* OspE protein promotes protein kinase C activation via PDLIM proteins. J. Biol. Chem 289, 30101–30113. [PubMed: 25124035]

Yoshida S, Handa Y, Suzuki T, Ogawa M, Suzuki M, Tamai A, Abe A, Katayama E, and Sasakawa C (2006). Microtubule-severing activity of *Shigella* is pivotal for intercellular spreading. Science 314, 985–989. [PubMed: 17095701]

Yum LK, Byndloss MX, Feldman SH, and Agaisse H (2019). Critical role of bacterial dissemination in an infant rabbit model of bacillary dysentery. Nat. Commun 10, 1826. [PubMed: 31015451]

Zychlinsky A, Kenny B, Ménard R, Prevost MC, Holland IB, and Sansonetti PJ (1994). IpaB mediates macrophage apoptosis induced by *Shigella flexneri*. Mol. Microbiol 11, 619–627. [PubMed: 8196540]

Highlights

- *Shigella flexneri* reduces membrane tension to promote intercellular spread
- The type 3 secretion protein IpaC is required for efficient protrusion formation
- IpaC interacts with β-catenin, altering the dynamics of adherens junctions

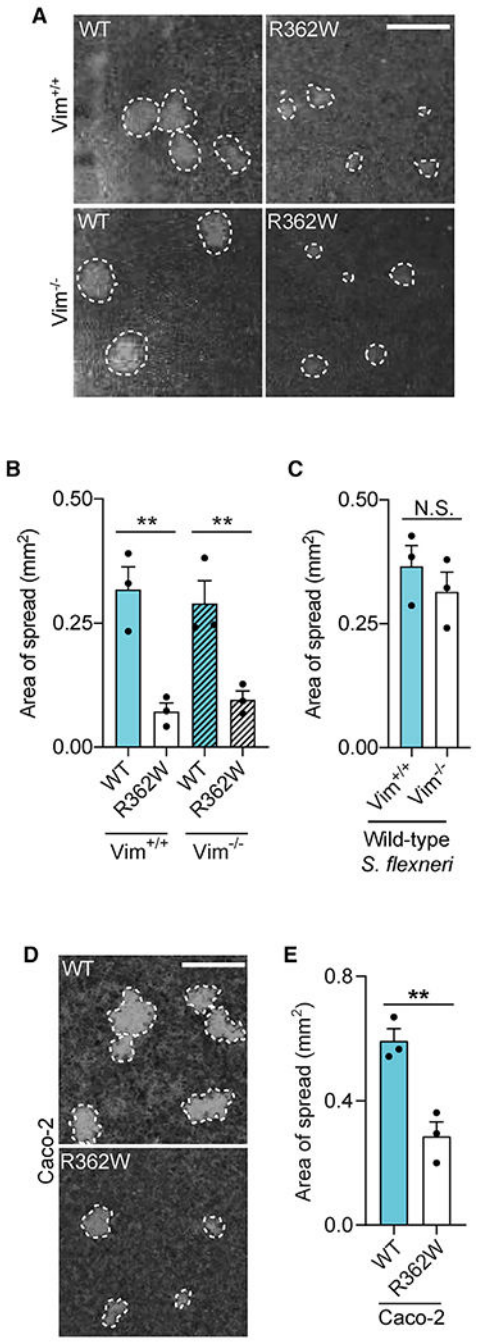

Figure 1. IpaC C-Terminal Tail Is Required for Efficient Intercellular Spread of *S. flexneri*

(A and B) Plaques formed in $Vim^{+/+}$ and $Vim^{-/-}$ MEF monolayers by *S. flexneri* Δ*ipaC*-producing WT IpaC (WT) or IpaC R362W (R362W). Representative images; 30–60 plaques measured per condition per experiment. (B) Plaque size from experiments represented in (A).

(C) Quantification of the size of plaques formed by WT *S. flexneri* in $Vim^{+/+}$ and $Vim^{-/-}$ MEFs. A total of 62–103 plaques were measured per condition per experiment.

(D) Plaques formed in Caco-2 monolayers by *S. flexneri* Δ*ipaC*-producing WT IpaC or IpaC R362W. Representative images; 30–56 plaques measured per condition per experiment. (E) Plaque size from experiments represented in (D). For bar graphs, dots represent independent experiments (B, C, and E); data are mean ± SEM. Scale bars, 500 μm. N.S., not significant; **$p < 0.01$; one-way ANOVA with Tukey post hoc test (B) or Student's t test (C and E). See also Figures S1 and S2.

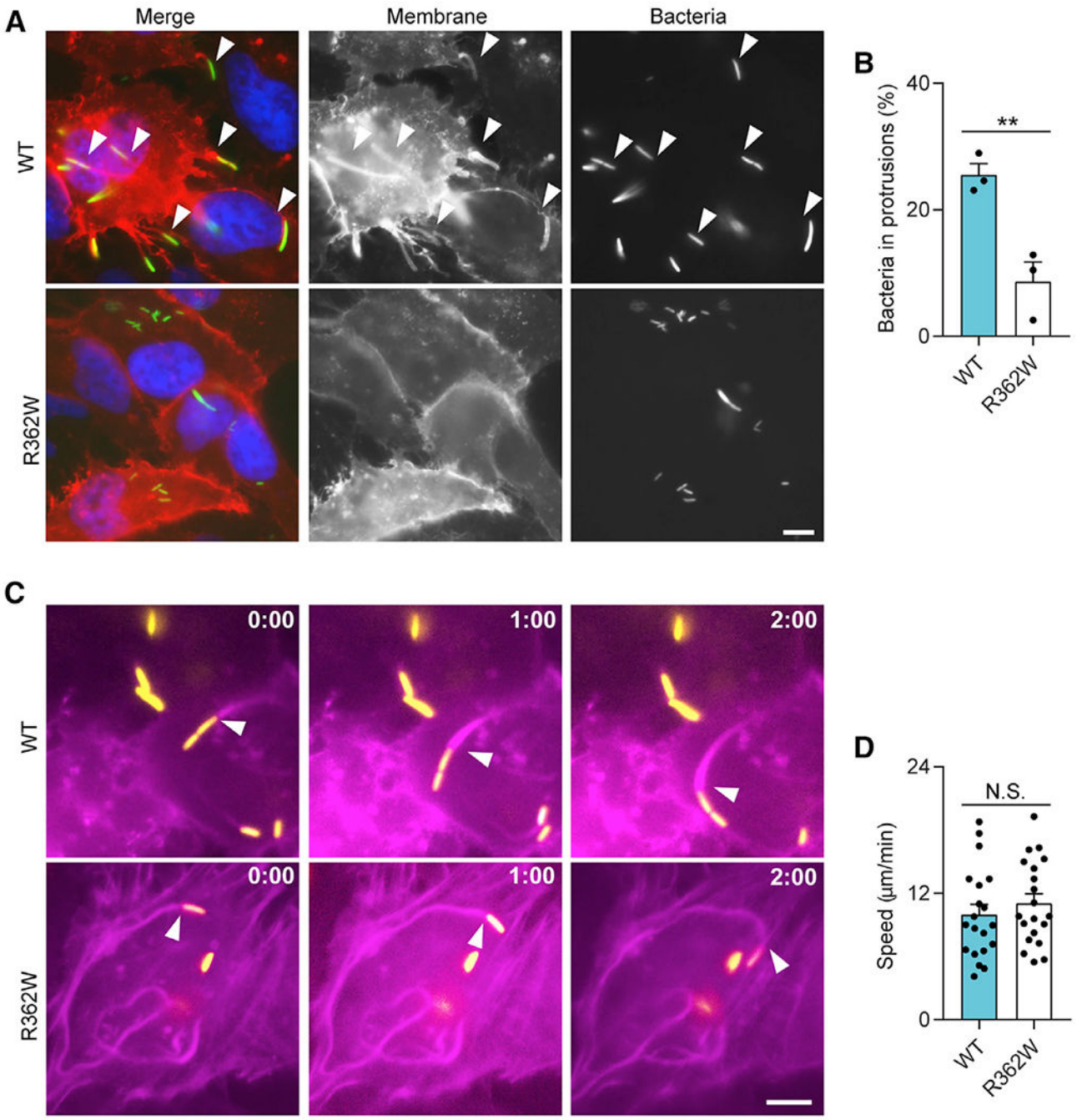

Figure 2. IpaC Is Required for Protrusion Formation by *S. flexneri*

(A) Plasma membrane protrusions formed in confluent HeLa cells by *S. flexneri* Δ*ipaC*-producing WT IpaC or IpaC R362W. Green, *S. flexneri*; red, t-farnesyl-red fluorescent protein (RFP), which labels plasma membranes; blue, DNA. Arrowheads, bacteria in protrusions. Representative images. Five random fields were analyzed per condition per experiment.

(B) Percentage of intracellular bacteria located within protrusions from (A), mean ± SEM.

(C) Live-cell imaging snapshots of actin-based motility of designated *S. flexneri* strains during infection of HeLa cells producing LifeAct GFP, which labels actin. Yellow, *S. flexneri*; purple, actin. Arrowheads, motile bacteria with unipolar polymerized actin. Representative images.

(D) Speeds of bacteria with polymerized actin at one pole, mean ± SEM. Ten bacteria imaged per condition per experiment. Data are from two (C and D) or three (A and B) independent experiments. Dots represent independent experiments (B) or individual bacteria(D). Scale bars, 10 μM. N.S., not significant; **$p < 0.01$; Student's t test. See also Figure S3.

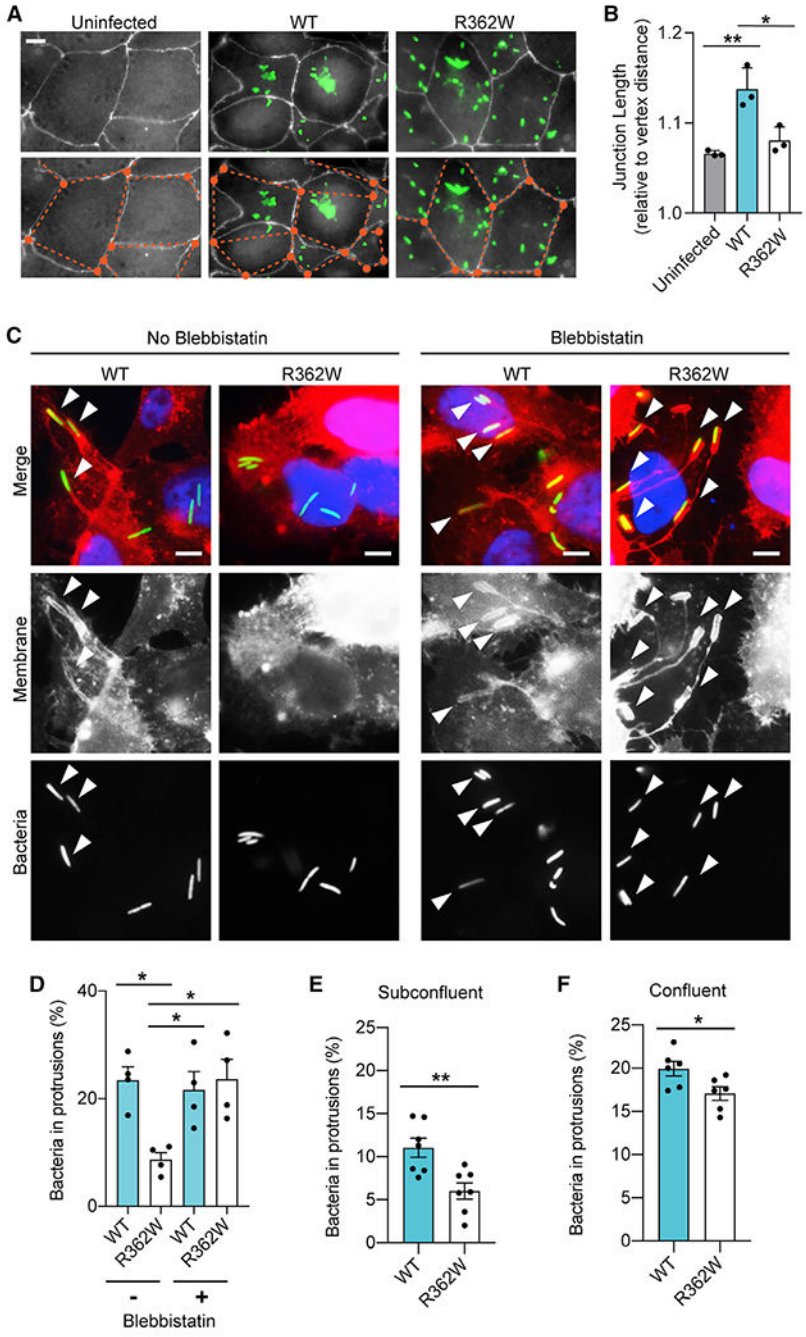

Figure 3. IpaC C-Terminal Tail Arginine Is Required for *S. flexneri*-Mediated Reduction of Host Membrane Tension.

(A and B) Infection of polarized Caco-2 cells with *S. flexneri* Δ*ipaC*-producing WT IpaC or IpaC R362W. (A) Cell-cell junctions of Caco-2 cells delineated by ZO-1 staining. White, ZO-1; green, *S. flexneri*; orange dots, membrane junctions; orange dashed lines, linear distances between junctions. Representative images. A total of 14–37 junctions were measured per condition per experiment. (B) Membrane length from (A), mean ± SEM. (C and D) Infection of HeLa cells by *S. flexneri* Δ*ipaC*-producing WT IpaC or IpaC R362W. (C) Plasma membrane protrusions formed in HeLa cells by *S. flexneri* Δ*ipaC*-producing WT

IpaC or IpaC R362W after treatment with blebbistatin or carrier. Arrowheads, bacteria in protrusions; red, t-farnesyl-RFP; green, *S. flexneri*; blue, DNA. Representative images. A total of 51–337 bacteria were analyzed per condition per experiment. (D) Percentage of bacteria in protrusions from (C), mean ± SEM.

(E and F) Infection of Caco-2 cells with *S. flexneri* Δ*ipaC*-producing WT IpaC or IpaC R362W. Quantification of the percentage of bacteria within protrusions in cells at the edge of a monolayer that are sub-confluent (E) or in cells that are confluent. (F). Five (E) or ten (F) fields were analyzed per condition per experiment. Dots represent independent experiments (B and D–F). Bars are mean ± SEM. Scale bars, 10 μM. *$p < 0.05$; **$p < 0.01$. One-way ANOVA with Tukey post hoc test (B and D) or Student's t test (E and F).

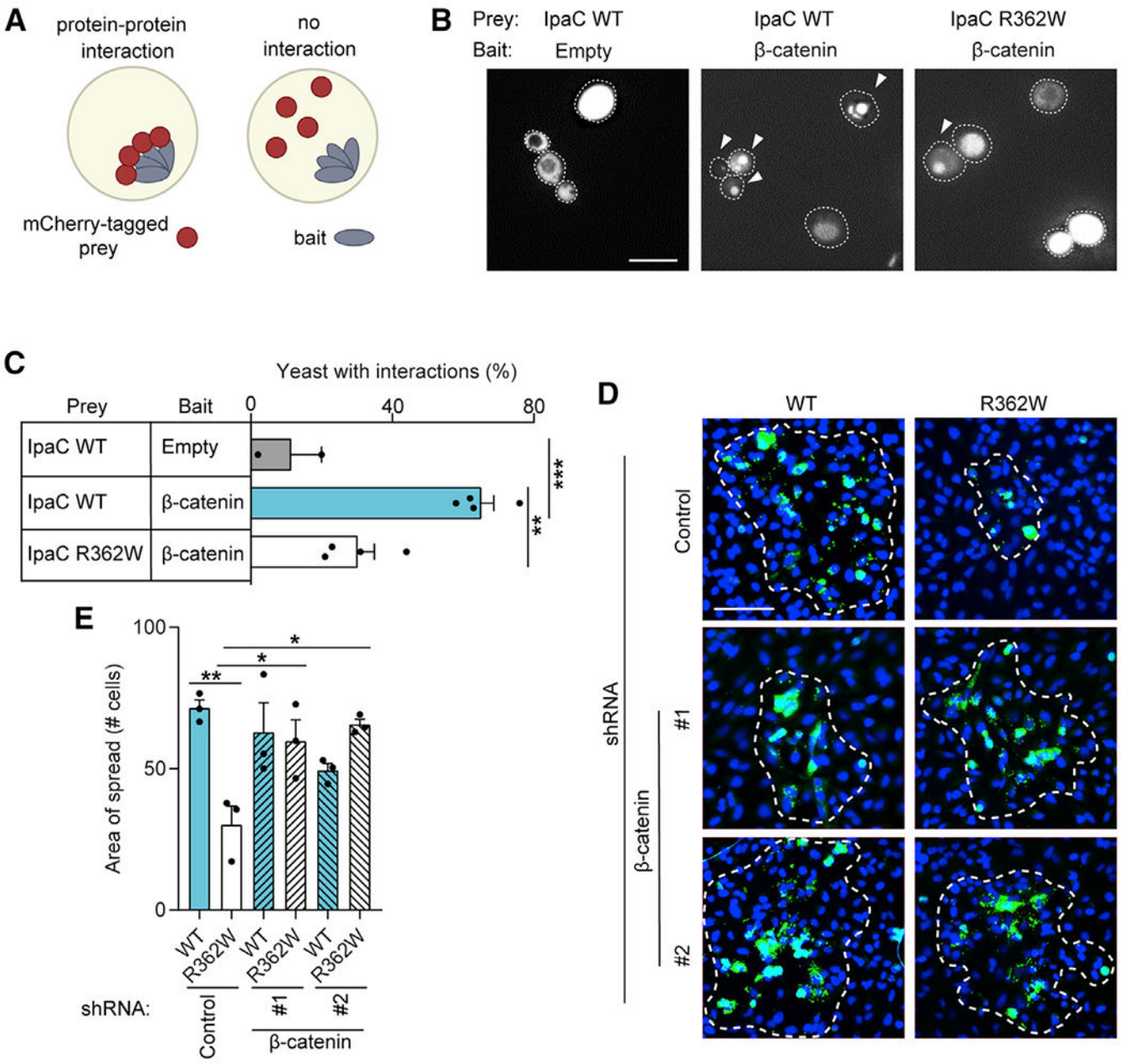

Figure 4. IpaC Interactions with β-Catenin Are Associated with *S. flexneri* Intercellular Spread

(A) Schematic of yeast protein-protein interaction platform. Interaction of the mCherry-tagged prey protein (red) with the bait protein fused to the inclusion body forming protein μNS (gray) results in puncta of red fluorescence. In contrast, the lack of an interaction between prey and bait proteins results in generally diffuse mCherry fluorescence throughout the cytosol of the yeast cells.

(B) Protein interaction assay. Arrowheads, fluorescent puncta. Representative images. A total of 88–186 yeast were analyzed per condition per experiment. Scale bar, 10 μM.

(C) Percentage of yeast displaying puncta, which indicates an interaction; mean ± SEM.

(D and E) Infection of HeLa cells with or without β-catenin knockdown by *S. flexneri* Δ*ipaC*-producing WT IpaC or IpaC R362W.

(D) Bacterial plaques formed in monolayers stably expressing β-catenin-targeting (#1 and #2) or control shRNA. Images collected at 18 h of infection. Green, *S. flexneri*; blue, DNA. Scale bar, 100 μm. Representative images. Five to ten fields were examined per condition per experiment.

(E) Quantification of plaque size (area of spread) from (D), mean ± SEM. Dots represent data from three or more independent experiments (C and E). *$p < 0.05$; **$p < 0.01$; ***$p < 0.001$; one-way ANOVA with Sidak post hoc test. See also Figure S4.

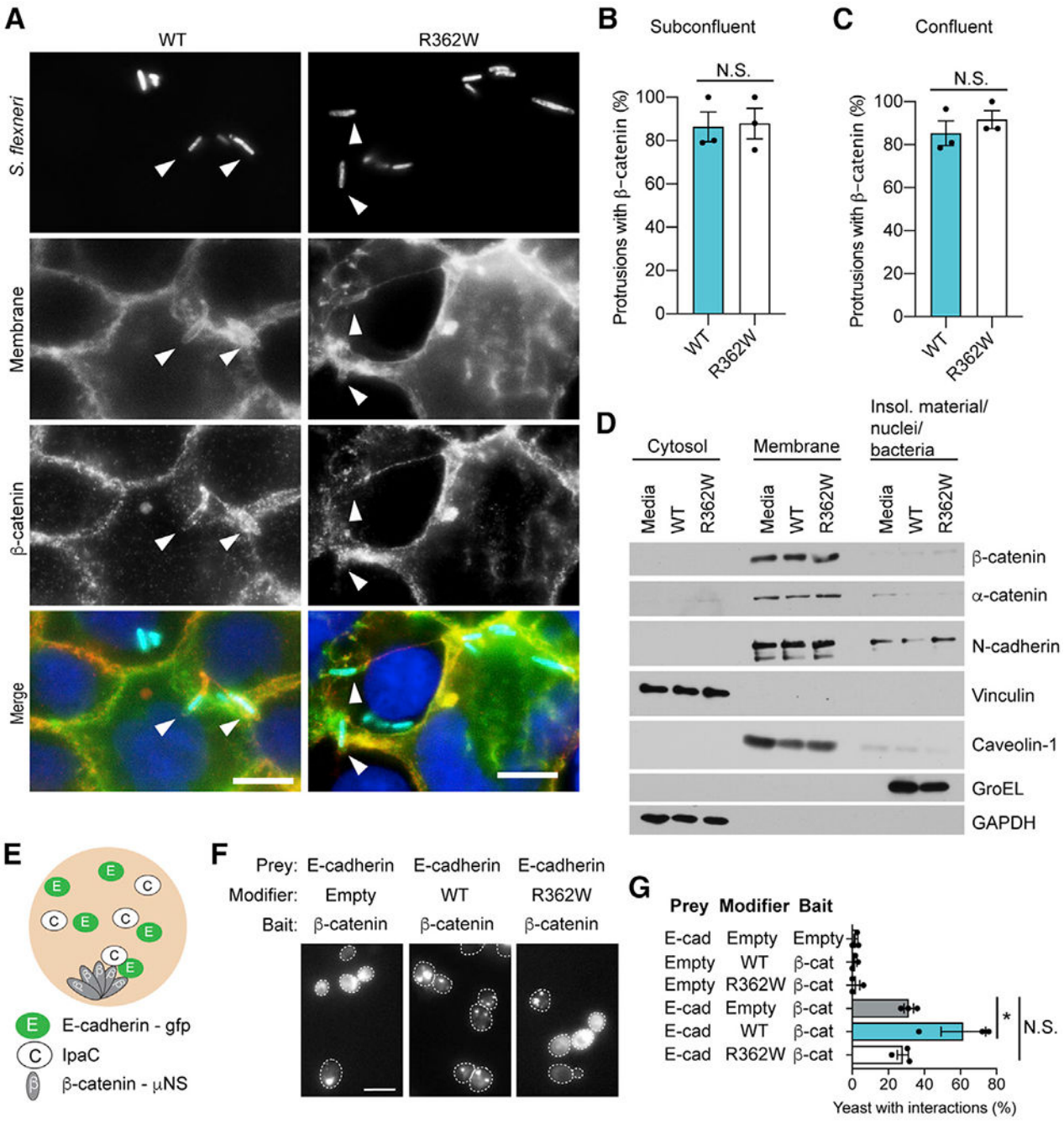

Figure 5. IpaC Stabilizes the β-Catenin-Cadherin Interaction

(A–C) Infection of Caco-2 cells with *S. flexneri*-producing WT IpaC or IpaC R362W. (A) Representative images. Five to ten images were analyzed per condition per experiment. Cyan, *S. flexneri*; green, membrane-bound YFP; red, β-catenin; blue, DNA. Scale bar 20 βM. (B and C) Quantification of the percentage of protrusions that colocalized with β-catenin in either sub-confluent (B) or confluent (C) cells. Student's t test. Data are mean ± SEM.

(D) Subcellular localization of β-catenin in HeLa cells infected with *S. flexneri*-producing WT IpaC or IpaC R362W.

(E–G) Yeast-based protein interaction assay comparing the efficiency of the interaction between β-catenin and E-cadherin in the presence of either WT IpaC or IpaC R362W. (E) Schematic showing prey is E-cadherin GFP, modifier is IpaC, and bait is β-catenin-μNS. (F) Representative images. Dotted lines are outlines of yeast. Scale bar, 10 μm. A total of 29–175 yeast were analyzed per condition per experiment. (G) Percentage of yeast displaying puncta, which indicates an interaction, from (F). Data are mean ± SEM. N.S., not significant. *$p < 0.05$; one-way ANOVA with Tukey post hoc test. See also Figure S5.

KEY RESOURCES TABLE

REAGENT or RESOURCE	SOURCE	IDENTIFIER
Antibodies		
Mouse anti-β-catenin	BD Biosciences	Cat #: 610153, RRID: AB_397554
Mouse anti-vinculin	Millipore Sigma	Cat#: SAB4200729; RRID: AB_2877646
Rat anti-N-cadherin	Developmental Studies Hybridoma Bank	Cat #: MNCD2, (Matsunami and Takeichi, 1995); RRID: AB_528119
Rat anti-E-cadherin	Thermo Fisher Scientific	Cat#: 14-3249-82; RRID: AB_1210458
Rabbit anti-α-catenin	Thermo Fisher Scientific	Cat#: 71-1200; RRID: AB_2533974
Rabbit anti-caveolin-1	Millipore Sigma	Cat#: C4490; RRID: AB_262110
Rabbit anti-GroEL	Millipore Sigma	Cat#: G6532; RRID: AB_259939
Mouse anti-GAPDH	Developmental Studies Hybridoma Bank	Cat#: DSHB-hGAPDH-2G7; RRID: AB_2617426
Rabbit anti-keratin 8	Abcam	Cat#: ab53280; RRID: AB_869901
Rabbit anti-keratin 18	Abcam	Cat#: ab668; RRID: AB_305647
Goat anti-rabbit HRP	Jackson ImmunoResearch Laboratories	Cat#: 111-035-144; RRID: AB_2307391
Goat anti-rat HRP	Jackson ImmunoResearch Laboratories	Cat#: 112-035-003: RRID: AB_2338128
Goat anti-mouse HRP	Jackson ImmunoResearch Laboratories	Cat#: 115-035-003; RRID: AB_10015289
Rabbit anti-Shigella-FITC	Virostat	Cat#: 0903; RRID: AB_2877645
Goat anti-rat Alexa Fluor 488	Thermo Fisher Scientific	Cat#: A-11006; RRID: AB_2534074
Goat anti-mouse Alexa Fluor 568	Thermo Fisher Scientific	Cat#: A-11004; RRID: AB_2534072
Rabbit anti-ZO1	Thermo Fisher Scientific	Cat#: 61-7300; RRID: AB_2533938
Goat anti-rabbit Alexa Fluor 594	Thermo Fisher Scientific	Cat#: A-11012; RRID: AB_2534079
HRP conjugated mouse anti-β-actin	Millipore Sigma	Cat#: A3854-200; RRID: AB_262011
Bacterial and Virus Strains		
Saccharomyces cerevisiae S288C	Gift of Cammie Lesser	N/A
Shigella flexneri strain 2457T	Lab Stock	Labrec et. al., 1964
S. flexneri 2457T Δ*ipaC*	Lab Stock	Russo et al., 2016
S. flexneri 2457T Δ*ipaC* pBAD33-WT IpaC	Lab Stock	Russo et al., 2016

REAGENT or RESOURCE	SOURCE	IDENTIFIER
S. flexneri 2457T Δ*ipaC* pBAD33- IpaC R362W	Lab Stock	Russo et al., 2016
S. flexneri 2457T Δ*ipaC* pBAD33-WT IpaC pTSAR	Lab Stock	Russo et al., 2016
S. flexneri 2457T Δ*ipaC* pBAD33- IpaC R362W pTSAR	Lab Stock	Russo et al., 2016
S. flexneri strain 2457T Δ*ipaC* pBAD33-WT IpaC pBR322-Afa-1	Lab Stock	Russo et al., 2019a
S. flexneri strain 2457T Δ*ipaC* pBAD33-IpaC R362W pBR322-Afa-1	Lab Stock	Russo et al., 2019a
S. flexneri 2457T Δ*icsB*	Lab stock	Baxt and Goldberg, 2014
S. flexneri 2457T Δ*ipaC* pBAD33-WT IpaC pROEX-Aqua	This Study	N/A
S. flexneri 2457T Δ*ipaC* pBAD33- IpaC R362W pROEX-Aqua	This Study	N/A
Chemicals, Peptides, and Recombinant Proteins		
InSolution Blebbistatin, Racemic	Calbiochem	203389
Gentamicin	Thermo Fisher Scientific	15750060
Neutral Red	Millipore Sigma	N2889
Hoechst 33342	Thermo Fisher Scientific	H3570
Fibronectin	Sigma	F1141
Alexa Fluor 568 Phalloidin	Thermo Fisher Scientific	A12380
Prolong Diamond	Thermo Fisher Scientific	P36965
Chloroquine	Millipore Sigma	C6628
Critical Commercial Assays		
Yeastmaker Yeast Transformation System 2	Takara	630439
Experimental Models: Cell Lines		
Mouse embryonic fibroblasts ($Vim^{+/+}$)	Gift of Victor Faundez	Styers et al., 2004
Mouse embryonic fibroblasts knocked out for vimentin ($Vim^{-/-}$)	Gift of Victor Faundez	Styers et al., 2004
HeLa CCL-2	ATCC	N/A
HeLa pCLIP2B-TFTR	This study	N/A
HeLa eGFP-LC3	Gift of Ramnik Xavier	Conway et al., 2013
HeLa LifeAct-GFP	This study	N/A
HeLa pLKO.1 + non-targeting shRNA	This study	N/A
HeLa pLKO.1 + β-catenin shRNA #1	This study	N/A
HeLa pLKO.1 + β-catenin shRNA #2	This study	N/A
Caco-2 Bbe2	Harvard Digestive Disease Center	N/A
Caco-2 pLKO.1 + non-targeting shRNA	This study	N/A
Caco-2 pLKO.1 + β-catenin shRNA #1	This study	N/A
Caco-2 pLKO.1 + β-catenin shRNA #2	This study	N/A
Caco-2 control knockdown	Lab stock	Russo et al., 2016
Caco-2 keratin 8 knockdown	Lab stock	Russo et al., 2016
Caco-2 keratin 18 knockdown	Lab stock	Russo et al., 2016

REAGENT or RESOURCE	SOURCE	IDENTIFIER
HEK293T	ATCC	Cat#: CRL-3216; RRID: CVCL_0063
Oligonucleotides		
β-catenin forward: CGAAGGAGATAGAACCATG GTTAAGCTCTTACACCCACCATCCC	IDT	N/A
β-catenin reverse: GGGGACAACTTTGTACAAGAAAGTTGG CAA CAG GTC AGT ATC AAA CCA GGC C	IDT	N/A
E-cadherin forward: CGAAGGAGATAGAACCatgagagcggtggtcaaagagc	IDT	N/A
E-cadherin reverse: GGGGACAACTTTGTACAAGAAAGTTGGgtcgtcctcgccgcctccgtacatg	IDT	N/A
Recombinant DNA		
pBY011-GFP	Gift of Cammie Lesser	Schmitz et al., 2009
pAG413-μNS	Gift of Cammie Lesser	Schmitz et al., 2009
pAG415-mCherry	Gift of Cammie Lesser	Schmitz et al., 2009
pAG415-mCherry-IpaC	Lab Stock	Russo et al., 2016
pAG413-μNS-β-catenin	This study	N/A
pBY011-GFP-E-cadherin	This study	N/A
pAG413-uNS-IpgC	Lab Stock	Russo et al., 2016
pLKO.1 - TRC scrambled control	Addgene	10879, (Moffat and Sabatini, 2006)
PLKO.1 -TRCN000314921 (β-catenin targeting #1)	The Broad Institute Genetic Perturbation Platform	Yang et. al., 2011
PLKO.1 - TRCN000314991 (β-catenin targeting #2)	The Broad Institute Genetic Perturbation Platform	Yang et. al., 2011
pVSVg	Addgene	12259
psPAX2	Addgene	12260
pmbYFP	Gift of Herve Agaisse	Weddle and Agaisse, 2018b
pCLIP2B-TFTR	Gift of Rebecca Lamason	Lamason et. al 2016
pROEX-Aqua	Addgene	42889
pTSAR	Gift of Claude Parsot	Campbell-Valois et. al., 2014
pBR322-Afa-1	Gift of Stanley Falkow	Labigne-Roussel et al., 1984
pBAD33-IpaC	Lab stock	Russo et al., 2016
pBAD33-IpaC R362W	Lab stock	Russo et al., 2016
Software and Algorithms		
GraphPad Prism 8	Graphpad Software	https://www.graphpad.com/scientific-software/prism/
Adobe Photoshop	Adobe	https://www.adobe.com/products/photoshop/photoshop/
Adobe Illustrator	Adobe	https://www.adobe.com/products/photoshop/photoshop/
ImageJ	NIH	https://imagej.nih.gov/ij/

REAGENT or RESOURCE	SOURCE	IDENTIFIER
IVision	BioVision Technologies	https://www.biovis.com/ivision.html